Design of an adaptive neuro-fuzzy computing technique for predicting flow variables in a 90° sharp bend

Azadeh Gholami, Hossein Bonakdari, Isa Ebtehaj and Ali Akbar Akhtari

ABSTRACT

Investigating flow patterns in sharp bends is more essential than in mild bends due to the complex behaviour exhibited by sharp bends. Flow variable prediction in bends is among several concerns of hydraulics scientists. In this study, the adaptive neuro-fuzzy inference system (ANFIS) is applied to predict axial velocity and flow depth in a 90° sharp bend. The experimental velocity and flow depth data for five discharge rates of 5, 7.8, 13.6, 19.1 and 25.3 L/s are used for training and testing the models. In ANFIS training, the two algorithms employed are back propagation (BP) and a hybrid of BP and least squares. In model design, the grid partitioning (GP) and sub-clustering methods are used for fuzzy inference system generation. The results indicate that ANFIS-GP-Hybrid predicts velocity best followed by flow depth.

Key words | 90° sharp bend, ANFIS model, back propagation, discharge, flow depth, velocity

Azadeh Gholami
Hossein Bonakdari (corresponding author)
Isa Ebtehaj
Ali Akbar Akhtari
Department of Civil Engineering,
Razi University,
Kermanshah,
Iran
E-mail: *bonakdari@yahoo.com*

INTRODUCTION

The presence of bends causes complex flow behaviour in rivers and open channels. Secondary and spiral flows are the main features in curved channels (Lien *et al.* 1999; Naji *et al.* 2010). The complex and three-dimensional nature of flow leads to change the velocity and water surface profile distribution (Ferguson *et al.* 2003; Zeng *et al.* 2008). Shukry (1950), Rozovskii (1961) and Anwar (1986) carried out the first extensive experimental studies on 90° and 180° sharp and mild bends. Rozovskii (1961) studied the flow properties and distribution of boundary shear stresses in curved channels with 90° mild bends and 180° sharp bends. Rozovskii also examined the location where the maximum velocity occurs and its displacement. He found that with mild bends, the maximum velocity displacement begins in the internal cross sections of the channel and is transmitted to outer walls because secondary flows overcome the pressure gradient. The velocity distribution and causes of secondary and spiral flows forming in bends were experimentally evaluated by Ye & McCorquodale (1998), Blanckaert & Graf (2001), Barbhuiya & Talukdar (2010) and Uddin & Rahman (2012). DeVriend & Geoldof (1983), Steffler *et al.* (1985), Bergs (1990) and Gholami *et al.* (2014) experimentally investigated transverse and longitudinal water surface profiles and slopes. In the numerical field, Leschziner & Rodi (1979), Bodnar & Prihoda (2006) and Ramamurthy *et al.* (2013) investigated the flow patterns in a 90° sharp bend and reported a nonlinear water surface slope. DeMarchis & Napoli (2006) numerically studied the distribution pattern of velocity components in a 270° bend. Their results indicated that the end section of the mild bend causes greater velocity at the outer channel wall than in other sections. Bonakdari *et al.* (2007) worked with a computational fluid dynamics (CFD) model to survey the bending effect on the velocity pattern in a channel with circular cross sections. Vaghefi *et al.* (2015) used the depth-averaged method to study and analyse the shear stress distribution near the bed in a 180° sharp bend. Gholami *et al.* (2014) experimentally and numerically investigated

doi: 10.2166/hydro.2017.200

the flow pattern in a 90° sharp bend with focus on the general flow characteristics. They evaluated the models' performance and found that sharp bends exhibit a full, three-dimensional, complex flow pattern.

In recent decades, artificial intelligence (AI) methods have become popular flow forecasting means in many engineering sciences. Numerous researchers have applied AI to solve an array of hydraulics problems, such as stream flow forecasting (Chiang *et al.* 2004; Chau & Wu 2010) and flow in open channels (Yuhang & Wenxin 2009; Gholami *et al.* 2015, 2016a, 2016b), and scour and sediment transport prediction (Liriano & Day 2001; Guven & Gunal 2008; Ebtehaj & Bonakdari 2013). AI methods are also frequently employed to predict the flow variables in curved channels. Sahu *et al.* (2011) used artificial neural network (ANN) modeling to study and predict the velocity values within a meander open channel. Bonakdari *et al.* (2011) predicted the velocity field values in a 90° mild bend using the multilayer perceptron neural network and genetic algorithm (GA). Their results indicated that the proposed networks are able to predict velocity values at points where experimental data are not available. Baghalian *et al.* (2012) examined ANN model performance and compared it with an analytical solution. They also studied a CFD model of the flow patterns in curved channels. According to their results, the multilayer perceptron (MLP) and CFD models predicted the flow pattern well.

More recently, fuzzy logic and neural networks have led to a novel neuro-fuzzy system called the adaptive neural fuzzy inference system (ANFIS). Asadiani Yekta *et al.* (2010) examined suspended sediment estimation using ANFIS, ANN and sediment rating curves. Their results showed that ANFIS is more accurate than ANN in estimating suspended sediment load as a discharge function. Samandar (2011) presented an ANFIS model to predict the friction coefficient of open channel flow. ANFIS modeling may be a suitable method of analysing general hydraulics problems that are mostly based on laboratory tests. Bahramifar *et al.* (2013) predicted the Manning roughness coefficient in alluvial channels using ANFIS. Moharana & Khatua (2014) applied ANFIS modeling to predict the roughness coefficient in meander open channel flow. The results signified that ANFIS modeling is a suitable and effective method of predicting the non-linear relationship between the roughness coefficient and effective non-dimensional factors. Ebtehaj & Bonakdari (2014) used ANFIS models with different training algorithms to predict sediment transport in sewers. By comparing the ANFIS models with theoretical equations, they concluded that ANFIS models can make more accurate predictions.

No study has been done on ANFIS in terms of evaluating the flow parameters in channel bends. Therefore, in this study, the velocity and water surface depth parameters of a 90° sharp bend were applied using the ANFIS method. In order to achieve FIS generation, sub-clustering (SC) and grid partitioning (GP) were employed and for model training, the back propagation (BP) algorithm and a hybrid of BP and least squares (LS) were used. As such, four different states (ANFIS-GP-BP, ANFIS-GP-Hybrid, ANFIS-SC-BP and ANFIS-SC-Hybrid) were applied in the current ANFIS design. Various network models were trained and tested based on extensive experiments in a 90° sharp flume. The velocity and water depth data were all related to five different discharge values. The inputs to each model were the coordinates (X and Y) of different points in the bend and discharge (Q) rate, and the outputs were velocity and flow depth, respectively.

METHODS

Experimental models

This experimental research was conducted in the hydraulic laboratory at Ferdowsi University of Mashhad using velocity and water depth data (Akhtari *et al.* 2009; Gholami *et al.* 2014). The channel had a 90° bend with one straight channel upstream (3.6 m) and a straight channel downstream (1.8 m). The cross section of the channel was square (40.3 × 40.3 cm width and flow depth), with a 90° bend central angle and average radius (R_c) of 60.45 cm. According to the channel width ($b = 40.3$ cm), the bend was sharp ($R_c/b = 1/5 < 3$). The channel bed and walls were fixed, smooth and made of Plexiglas. Flow at five different values entered the flume at water depths of 4.5, 6, 9, 12 and 15 cm. A one-dimensional velocity meter (propeller)

read the axial velocities in the flume with 2 cm/s precision and a micrometre measured the water depth with 0.1 mm precision. The velocity meter was placed by vernier ruler in the transverse direction with 0.5 mm accuracy and by analog caliper in the depth direction with 0.1 mm accuracy. The propeller measured the velocity in the flow direction (axial velocity or radial velocity). Inside the bend cross sections (e.g. 22.5°, 45° and 67.5° cross sections), the propeller recorded the flow velocity in the channel axis direction as well. To find the velocity in the longitudinal and transverse directions in the internal cross sections (e.g. 45°), the radial velocity gained by the propeller was split in the X and Y directions. The different hydraulic flow characteristics are given in Table 1. In each of the five cases, the flow regime was subcritical and turbulent. The channel's geometric properties are presented in Figure 1.

Table 1 | Different hydraulic experimental characteristics

Number of test	Normal depth, H_o (m)	Discharge, Q (m³/s)	Velocity, V (m/s)	Froude Number, Fr	Reynolds Number, Re
1	0.045	0.005	0.273	0.42	12,460
2	0.06	0.0078	0.321	0.42	18,460
3	0.09	0.0136	0.374	0.40	28,940
4	0.12	0.0191	0.394	0.36	36,860
5	0.15	0.0253	0.419	0.34	44,705

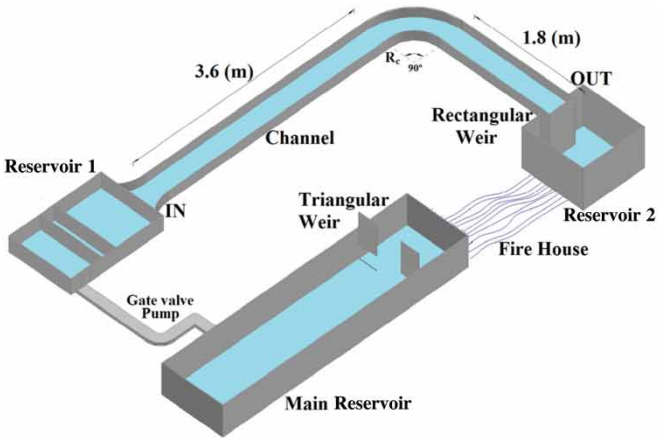

Figure 1 | Experimental model geometry.

Equation for bends suggested based on dimensional analysis

If the non-dimensional parameters are defined as $P_{d-r}, \ldots, P_3, P_2, P_1$, the relation (based on the Buckingham theory) between these parameters is determined as:

$$F(P_1, P_2, P_3, \ldots, P_{d-r}) = 0.0 \tag{1}$$

In the present study, the independent initial variables are water surface depth variation (ΔH), average flow velocity (V), gravitational acceleration (g), channel's central axis radius (R_c), channel width (b) and normal flow depth (H_0). According to the Buckingham theory, if there are d variables with r main dimensions in one problem, the $d-r$ independent non-dimensional parameters can be defined. Hence, in the present problem, there are $d=6$, $r=2$ and $d-r=4$ non-dimensional P factors. The following power equation is considered for relating the previously dimensionless values as:

$$\frac{\Delta H}{b} = \left(\frac{v^2}{R_c.g}\right)^{\alpha} \cdot \left(\frac{H_0}{b}\right)^{\beta} \cdot \left(\frac{R_c}{b}\right)^{K} \tag{2}$$

Since the present case study bend is a sharp bend with $R_c/b = 1.5$, the mentioned ratio variations cannot be considered; thus, the above relation changes to:

$$\frac{\Delta H}{b} = \left(\frac{v^2}{R_c.g}\right)^{\alpha} \cdot \left(\frac{H_0}{b}\right)^{\beta} .k \tag{3}$$

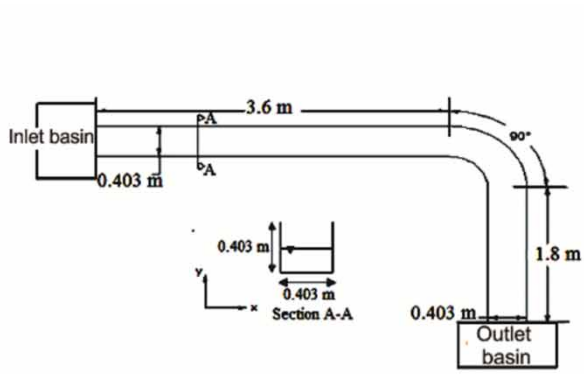

Table 2 | Averaged flow depth variation values at each discharge in a 90° bend

The normal depth, H_0 (m)	Flow discharge, Q (m^3/s)	Flow velocity, V (m/s)	The measured flow depth variations, ΔH (m)
0.045	0.005	0.273	0.0067
0.06	0.0078	0.321	0.0093
0.09	0.0136	0.374	0.0127
0.12	0.0191	0.394	0.0135
0.15	0.0253	0.419	0.0152

Table 2 shows the averaged values of transverse water surface depth variations, the normal depth and the averaged flow velocity at each discharge in the 90° bend. The above equation parameters are calculated using data from Table 2. Finally, Equation (4) is suggested for calculating flow depth variations in a 90° bend:

$$\Delta H = 0.4167.\, b.\left(\frac{v^2}{R_c.g}\right)^{0.5905}.\left(\frac{H_0}{b}\right)^{0.3205} \quad (4)$$

ANFIS

A fuzzy system is based on if-then logic rules and cannot be analysed using the classical probability theory. To begin fuzzy system construction, a set of if-then rules must be achieved. Consequently, a method should be available to use the existing information in order to determine if these rules are considered an efficient tool. Owing to the different training capabilities, a neural network is able to create appropriate links between the input and output variables. Therefore, a FIS and neural network combination known as an ANFIS can serve as a powerful tool to solve various problems. In this method, the fuzzy part creates the relationship between the input and output variables and the fuzzy membership function parameters are optimized by the neural network. ANFIS was first introduced by Jang (1993). The network structure used in this study with three inputs X, Y and Q is given in Figure 2. The values of the three parameters are supplied by the three input nodes and the output value obtained is transferred via membership functions (MFs).

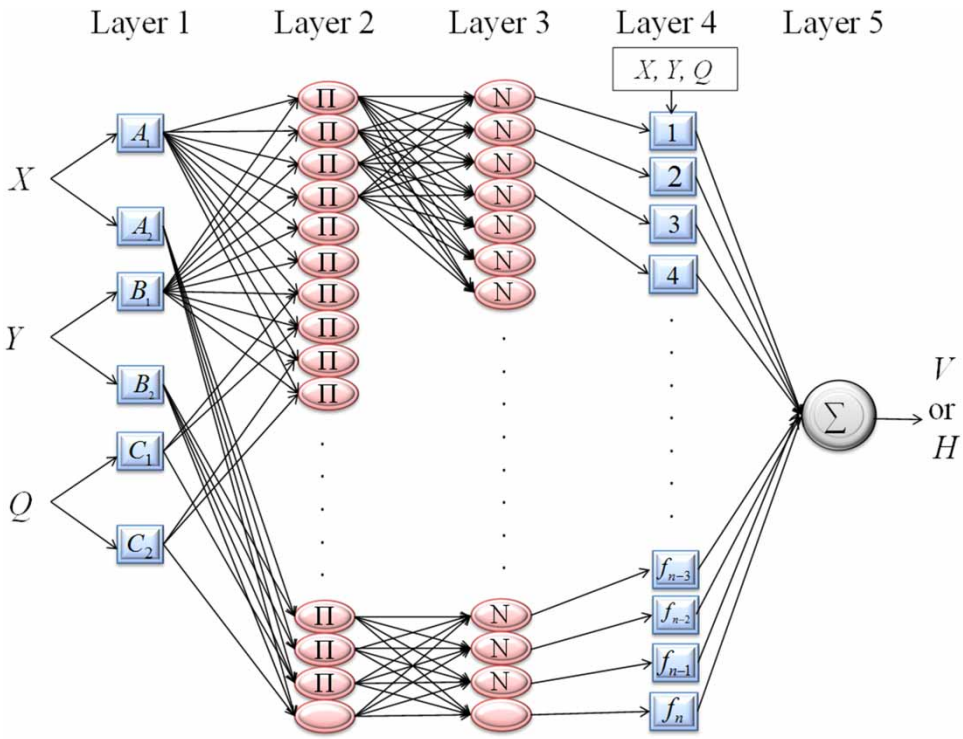

Figure 2 | The ANFIS network used in this study.

The adequate Gaussian membership function performance in many practical studies is due to this function's smoothness and concise notation effect. The MFs employed in this study are the Gaussian type and are calculated using Equation (5):

$$\mu_{M_i}(X) = exp\left(-\frac{\|X - c_i\|^2}{2\sigma_i^2}\right) \tag{5}$$

where $\{c_i$ and $\sigma_i\}$ is the changeable premise parameter set and μ is the MF. Similarly, this method is also used to calculate the Y input. After calculating the MFs, their values are multiplied in the next layer using Equation (6):

$$w_i = \mu_{M_i}(X)\mu_{N_i}(Y)\mu_{T_i}(Q) \qquad (i = 1, 2, 3) \tag{6}$$

The output of the above equation is known as a firing strength rule. The normalized firing strength is calculated as:

$$\overline{w_i} = \frac{w_i}{\sum w_i} \qquad (i = 1, 2, 3) \tag{7}$$

In the next layer, a weighted factor (Equation (7)) is used to calculate the ith rule portion from the total output:

$$\textit{If } X \textit{ is } M_1,\ Y \textit{ is } N_1 \textit{ and } Q \textit{ is } T_1,\ \textit{Then } f_1(X, Y, Q) = p_1X + q_1Y + s_1Q + r_1 \tag{8}$$

$$\overline{w_i}f_i = \overline{w_i}(p_iX + q_iY + s_iQ + r_i) \tag{9}$$

where $\{p_i, q_i, s_i$ and $r_i\}$ is the changeable consequent parameter set. In the final stage, the sum of all input signals is presented as the network output (V or H). The final ANFIS output is calculated as follows:

To examine the FIS generation in this study, the GP and SC methods are used. The performance of each method is expressed next.

GP

In this approach, the input space is apportioned in several rectangular subspaces using a number of fuzzy regions. The space partitioning is achieved based on the type and number of MFs in each dimension by the portion parallel to the axis. To determine the fuzzy sets and parameters, the LS approach according to the membership function type and partition is utilized. It should be noted that the consequent parameters related to the linear output of the membership function are set to zero during the production of fuzzy rules. Subsequently, the parameters are determined and refined by ANFIS. The ANFIS and GP combination was presented by Kennedy *et al.* (2003) in detail. The number of fuzzy rules is exponentially dependent on the number of input parameters. By considering that the number of input parameters and the membership function for each parameter are m and n, the whole number of fuzzy rules is equal to m^n. Therefore, GP is not suitable for problems with large numbers of input variables (Jang 1993). The number of input variables in this study is equal to 3 (X, Y, Q), which allows using GP in FIS generation.

SC

The SC approach is an extension of mountain clustering (Yager & Filev 1994). In this method, data points are utilized in GP instead of grid points, and each data point can be considered a potential cluster center. The effective grid point that must be evaluated is independent of the problem dimension and is equal to the number of data points. Furthermore, this technique does not require specifying the grid resolution, where tradeoffs between accuracy and computational complexity would have to be taken into account. The SC process is presented as follows.

$$\begin{aligned} f(V \text{ or } H) = \sum_i \overline{w_i}f_i = \frac{w_1}{w_1 + w_2}f_1 + \frac{w_2}{w_1 + w_2}f_2 + \frac{w_3}{w_1 + w_2}f_3 = \overline{w}_1(p_1X + q_1Y + s_1Q + r_1) + \overline{w}_2(p_2X + q_2Y + s_2Q + r_2) \\ + \overline{w}_3(p_3X + q_3Y + s_3Q + r_3) = (\overline{w}_1X)p_1 + (\overline{w}_1Y)q_1 + (\overline{w}_1Q)s_1 + (\overline{w}_1)r_1 + (\overline{w}_2X)p_2 + (\overline{w}_2Y)q_2 \\ + (\overline{w}_2Q)s_2 + (\overline{w}_2)r_2 + (\overline{w}_3X)p_3 + (\overline{w}_3Y)q_3 + (\overline{w}_3Q)s_3 + (\overline{w}_3)r_3 \end{aligned} \tag{10}$$

Consider a set of N data points $\{x_1, x_2, x_3, \ldots, x_n\}$ in M dimensions, which have been normalized in each dimension and bounded using a unit hypercube. The potential of each data point (x_i) that can be considered a potential cluster center is calculated as follows:

$$P_i = \sum_{i=1}^{N} e^{-\alpha \|X_i - X_j\|^2} \tag{11}$$

Here, α is equal to $4/r_a^2$, where r_a is a positive constant defining a neighborhood and $\|X_i - X_j\|^2$ shows the Euclidean distance. Based on the above equation, the potential of each data point is dependent on its distance to other data points. Therefore, if one data point has many neighboring data points, it would have a high potential value, and the data points outside the r_a radius would have little impact on the potential. The first cluster center is selected by a data point with the highest potential. If x_1^* and P_1^* are the location and potential value of the first cluster center (respectively), the potential of each data point (x_i) is calculated as follows:

$$P_i \Leftarrow P_i - P_1^* e^{-\beta \left\| X_i - X_j^* \right\|^2} \tag{12}$$

Here, β is equal to $4/r_b^2$, where r_b is a positive constant that defines the neighborhood radius effectively. Thus, an amount of the potential of each data point is subtracted. The data points nearest to the center of the first cluster considerably reduce the potential and are improbable to be selected as the next cluster center. To prevent achieving closely spaced cluster centers, r_b should be considered greater than r_a, such that $r_b = 1.25 r_a$ as proposed by Chiu (1997). After revising the potential of all data points based on Equation (12), the data point with the highest potential is selected as the second cluster center. After selecting the k^{th} cluster center, the potential of each data point is calculated using the following equation:

$$P_i \Leftarrow P_i - P_{k1}^* e^{-\beta \|X_i - X_k^*\|^2} \tag{13}$$

where x_k^* and P_k^* are the location of the k^{th} cluster center and its potential, respectively.

The procedure of obtaining a new cluster center and revising the potential of each is repeated until the residual potential of all data points is lower than some deduction of the first cluster center's potential (P_1^*).

The influential radius value is directly dependent on the amount of rules, such that a small radius results in small clusters and a higher number of rules and vice versa. Consequently, the influential radius needs to be properly selected for data space clustering. The algorithms applied for training include BP and a hybrid of BP and LS. Thus, the ANFIS network design has four different states. The network inputs include X, Y and Q (longitudinal and transverse coordinates and discharge, respectively). A single output is considered, either the velocity or flow depth parameter. As a result, eight different models are presented in this study.

Bowden *et al.* (2002) optimized the data used for ANN model training and testing by two methods: the GA and self-organizing map (SOM). GA was applied to a problem of dividing the data into three statistically similar subsets. The SOM technique achieves an equally distributed training set by first dividing all data into a number of classes. Then by sampling an equal number of records from each cluster, the training, testing and validation set data are distributed throughout the problem domain equally. Bowden *et al.* (2002) stated that the poor performance of the ANN model was related to their own data and not the choice of ANN model parameters or architecture. The two mentioned methods reduced the prediction error pertaining to the conventional data division method. The method for data selection was such that from 520 velocity data, 400 were used for model training (75%) and the remaining 25% (120 data) were used for model performance testing. From 506 different flow depth data, 386 were employed for model training and 120 for model testing.

RESULTS AND DISCUSSION

Data analysis

In this article, eight different ANFIS models are used to predict the velocity and flow depth in a 90° sharp bend. To predict the flow depth and velocity, the point coordinates in two directions (X, Y) and the discharge (Q) served as input parameters and flow depth and velocity were the output parameters. The experimental velocity and flow depth values at five discharges of 5, 7.8, 13.6, 19.1 and 25.3 L/s were used. The propeller recorded axial velocity in the flow direction. The experimental depth and velocity data of eight cross

sections (40 cm after the bend, 0°, 22.5°, 45°, 67.5°, 90°, and 40 and 80 cm after the bend) and 13 points in each cross section were used to train and test the ANFIS models. The experimental data related to four distances ($Z = 0.03$, 0.06, 0.09 and 0.12 m) from the channel bed were used for velocity prediction. Figure 3 shows a three-dimensional view of eight channel cross sections in plan for a 90° bend, where the velocity values and 13 transverse points in each cross section were measured experimentally.

Model evaluation

In the present study, the performance of four different ANFIS models, i.e. GP-Hybrid, GP-BP, SC-Hybrid and SC-BP, is examined by applying the coefficient of determination (R^2), root mean square error (*RMSE*), mean absolute percentage of error, scatter index (*SI*) and *bias* (Equations (14)–(18)):

$$R^2 = 1 - \frac{\sum_{i=1}^{N} (Y_{i(model)} - Y_{i(Observed)})^2}{\sum_{i=1}^{N} (Y_{i(model)} - \bar{Y}_{i(model)})^2} \quad (14)$$

$$RMSE = \left[\frac{\sum_{i=1}^{N} (Y_{i(model)} - Y_{i(Observed)})^2}{N} \right]^{0.5} \quad (15)$$

$$MARE = \frac{1}{N} \sum_{i=1}^{N} \left(\frac{|Y_{i(model)} - Y_{i(Observed)}|}{Y_{i(Observed)}} \right) \quad (16)$$

$$Bias = \frac{\sum_{i=1}^{N} (Y_{i(model)} - Y_{i(Observed)})}{N} \quad (17)$$

$$SI = \frac{RMSE}{(1/N) \sum_{i=1}^{N} Y_{i(Observed)}} \quad (18)$$

where $Y_{i(Observed)}$ is the output observational parameter, $Y_{i(\mathrm{model})}$ is the parameter predicted by the ANFIS models, $\overline{Y}_{i(\mathrm{model})}$ is the mean ANFIS model parameter and N is the number of parameters. The absolute error index of *RMSE* has the benefit that its results have the same experimental model scale and units. In high flow ranges, the *RMSE* value provides a good measure of model efficiency. The comparison between actual and estimated values is done by the relative error value of *MARE*. This index shows the accuracy criterion of level prediction. It is an unbiased statistic for measuring the predictive capability of a model. *MARE* is a relative criterion that is sensitive to the forecasting errors that

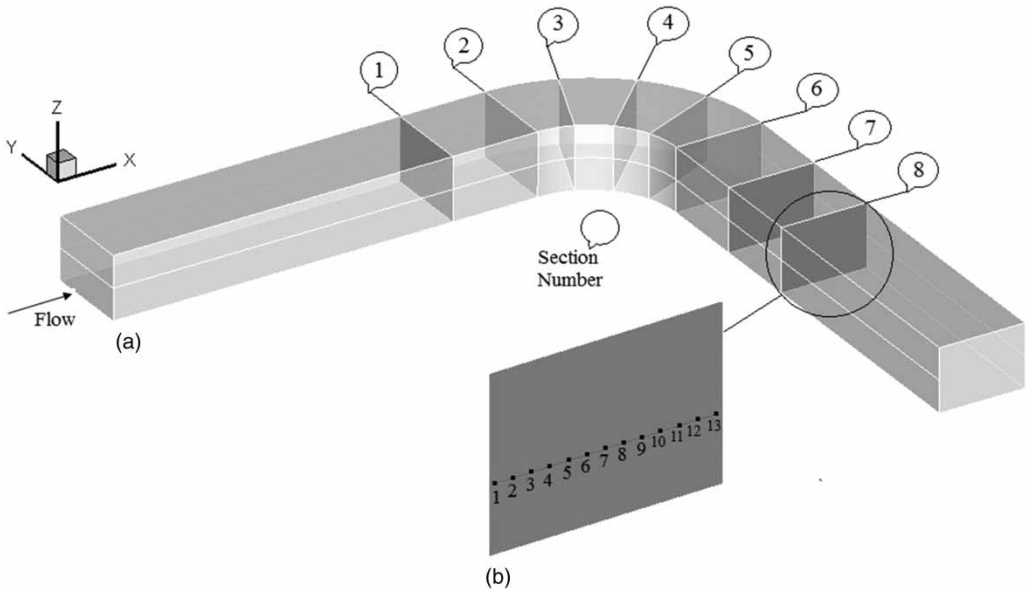

Figure 3 | (a) 3D view of cross sections; (b) 13 transverse points in the cross sections.

occur at low magnitudes of each dataset and is less sensitive to the larger errors that usually occur at higher magnitudes because the errors are not squared (Wang *et al.* 2015). The ideal *RMSE* and *MARE* values are zero, with index values closer to zero indicating greater model accuracy. The coefficient of determination (R^2) is the linear regression line between the values predicted by the ANFIS models and the observation values utilized to determine the network application. R^2 is a criterion that illustrates how well the ANFIS data fit the experimental data. The SI is a normalized measure of error that takes into account the observed data. Lower *SI* values are an indication of better forecasting.

Evaluation of velocity prediction models

In Figure 4, the regression curves of actual and velocity data predicted by the four models are plotted with respect to the testing and training datasets. More data were used for network training than for testing. In these graphs, the velocities are non-dimensional values. As such, the velocities obtained by the ANFIS models are divided into the maximum velocity values at each discharge (V/V_{max}). According to the figure, most data scattering occurred with the testing dataset. All four models' prediction accuracy declined at low velocity and increased at higher velocity values. The SC-BP and SC-Hybrid models exhibited the same functionality and prediction accuracy.

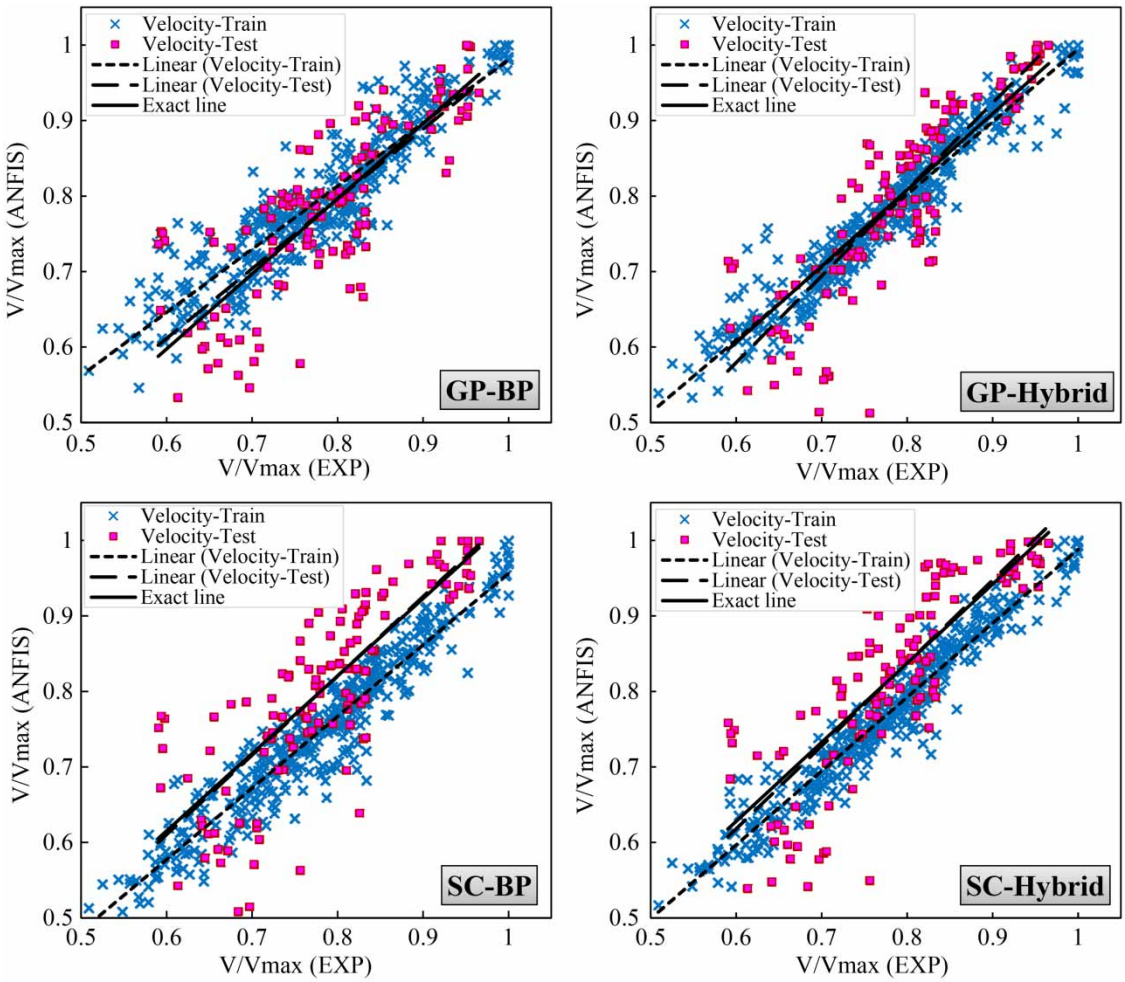

Figure 4 | Regression graphs of the velocity values predicted by the GP-Hybrid, GP-BP, SC-Hybrid and SC-BP models compared with the experimental results for the training and testing datasets.

With the GP-Hybrid model, data compression around the fitted line was greater than the other models, and it can thus be concluded that GP-Hybrid predicted velocity more accurately. It is not obvious which model was more accurate from these figures. Therefore, Table 3 shows the statistical indices for the GP-Hybrid, GP-BP, SC-Hybrid and SC-BP models with the training and testing datasets. The training stage was more accurate than the testing stage. However, there is no significant difference between the results from the two stages, and in the worst condition the SC-Hybrid model's accuracy (R^2 value) decreased by 16% in the testing stage. The table demonstrates that the GP-hybrid model has the highest R^2 error index value compared with the other models. The high R^2 value indicates the good agreement between the values predicted by this model and experimental data. The lower *RMSE* and *SI* index values for the GP-BP model are obvious, but the nearly equal values for these indices to GP-Hybrid represent the similar nature of these two models.

However, GP-Hybrid is introduced as the superior model owing to the higher R^2 and *MARE* (0.867 and 0.076, respectively) than the GP-BP model. The relative error index of *MARE* increased by nearly 6% by changing the FIS generation method to SC, meaning that the SC-Hybrid model was less accurate than the GP-Hybrid model. In the GP-Hybrid model, however, by changing both the FIS generation method and training algorithm, the *MARE* error index increased by 12%. Hence, the SC-BP model was less accurate in predicting the velocity parameter due to the high *SI* error index ($SI = 0.099$). Therefore, it can be said that the GP generation method is more accurate than the SC method. Moreover, for both generation methods (GP and SC), using hybrid models is better than the BP training algorithm. The positive and negative *bias* index values also indicate the overestimation and underestimation of these models, respectively. According to the negative and positive values in Table 3, it can be said that the GP-BP and GP-Hybrid models underestimated and overestimated, respectively.

As a result, the GP-Hybrid model is considered the most accurate in velocity prediction. In the grid-partitioning model for FIS generation with the training hybrid algorithm, the R^2 value in both stages (training = 0.968, testing = 0.867) was the highest. In training, the GP-Hybrid model had the lowest error values ($RMSE = 1.378$, $MARE = 0.027$) compared with the other models. The *bias* and *SI* values for this model were 0.079 and 0.09, respectively.

Evaluation of water surface depth prediction models

Four models, i.e. GP-Hybrid, GP-BP, SC-Hybrid and SC-BP were designed separately to predict water depth. The evaluation of the four models using different statistical indices for the training and testing datasets is shown in Table 4. Evidently, all models had the same R^2 value and the same function; hence, in this study, different discharge rates (different water depths) were considered as input parameters and the results of each ANFIS model are given in terms of total discharge.

Table 3 | Evaluation of the GP-Hybrid, GP-BP, SC-Hybrid and SC-BP models in velocity prediction using various indices for the training and testing datasets

Model type	R^2	RMSE	MARE	Bias	SI
Training datasets					
GP-BP	0.923	2.051	0.044	−0.049	0.053
GP-Hybrid	0.968	1.378	0.027	0.333	0.036
SC-BP	0.95	1.72	0.038	−1.07	0.044
SC-Hybrid	0.965	1.45	0.03	−0.7	0.037
Test datasets					
GP-BP	0.856	3.377	0.077	−0.71	0.087
GP-Hybrid	**0.867**	**3.5**	**0.076**	**0.795**	**0.09**
SC-BP	0.82	3.844	0.085	1.618	0.099
SC-Hybrid	0.83	3.731	0.081	1.528	0.096

Table 4 | Evaluation of the GP-Hybrid, GP-BP, SC-Hybrid and SC-BP models in flow depth prediction using various indices for the training and testing datasets

Model type	R^2	RMSE	MARE	Bias	SI
Training datasets					
GP-BP	0.998	0.166	0.02	0.077	0.018
GP-Hybrid	0.999	0.042	0.003	0.0067	0.0045
SC-BP	0.999	0.108	0.011	−0.083	0.012
SC-Hybrid	0.999	0.116	0.0129	−0.104	0.0126
Test datasets					
GP-BP	0.997	0.224	0.028	−0.167	0.024
GP-Hybrid	**0.998**	**0.155**	**0.02**	**−0.107**	**0.017**
SC-BP	0.998	0.16	0.02	−0.121	0.017
SC-Hybrid	0.998	0.162	0.02	−0.131	0.0173

Similar to the velocity prediction models, GP-Hybrid had lower error values in the testing stage ($RMSE = 0.155$, $MARE = 0.02$) and outperformed the other models. Moreover, the *bias* and *SI* indices of 0.107 and 0.017 respectively, of this model were lower than the comparable values of the other model. The GP-Hybrid model predicted water depth in a 90° bend reasonably well.

By changing the training algorithm from hybrid to BP, the model error increased and the GP-BP model had the greatest relative and absolute errors (*RMSE*, *MARE* and *SI* of 0.022, 0.028 and 0.024, respectively) and was thus introduced as the least accurate model for water surface depth prediction. By changing the generation method from GP to SC, the SC-BP and SC-Hybrid models' relative error (*MARE*) slightly increased by 3.5% and 4.5%, respectively, but SC-BP (with $SI = 0.0170$) was more accurate than the SC-Hybrid model ($SI = 0.0173$). Therefore, it can be said that unlike the velocity prediction models, the SC-BP model with *MARE* index of 0.16 ranks second after the GP-hybrid model in terms of flow depth prediction accuracy; the SC-BP model performed similar to the GP-Hybrid model with equal *MARE* and *SI* error index values. The negative *bias* index values for the four models indicate underestimation, especially from the two SC models, due to the negative *bias* index values in the training stage.

Figure 5 illustrates scatter plots of the flow depth values predicted by the GP-Hybrid model versus experimental data at different discharge rates (the water depth prediction results for five different discharge rates versus experimental values are plotted separately, but all five discharges correspond to the GP-hybrid model results and only the results are separate). In these graphs, the flow depth values are dimensionless. The non-dimensional values were obtained by dividing the flow depths predicted by the ANFIS models by the maximum flow depth at each discharge (H/H_{max}). It is obvious from these figures that the GP-BP model with the highest R^2 (0.83) at 19.1 L/s discharge was the most accurate. It can also be concluded that this model was more accurate at higher than lower discharge rates. With a discharge increase from 5 to 25.3 L/s, the R^2 value also increased for the training and testing datasets.

Velocity contours

In the sections before the bend the flow velocity distribution is uniform, similar to straight channels. As flow enters the bend, the maximum velocity occurs at the inner channel wall. By advancing into the bend and with the power of secondary flows, the maximum velocity gradually transmits to the channel axis and transfers to the outer wall in the cross sections located after the bend. In the sections after the bend, the flow velocity is not yet uniform and the maximum velocity is at the outer channel wall. In the sections after the bend, the velocity profiles will be uniform after flow establishment length. However, during the experiments, the mean velocity profiles 20–30 cm before and 150–160 cm after the bend remained constant and a fully developed zone (establishment length) was achieved in our experiments. Rozovskii (1961) stated that the main factor behind velocity displacement in mild bends is secondary flows, while in sharp bends it is the longitudinal pressure gradient; therefore the establishment length in mild bends is more important than in sharp bends, due to the power of secondary flows. He offered a relation for determining a specific length when the secondary flow has maximum strength. Based on this relation, he concluded that in order for secondary flow to develop, there needs to be a bend with a central angle of at least 100° for shallow flumes, and a 180° central angle for deep flumes. He also observed that the logarithmic distribution probability for velocity profiles leads to favourable results.

The maximum velocity always remains at the inner wall in sharp bends, unlike mild bends (Rozovskii 1961; Leschziner & Rodi 1979; Naji *et al.* 2010). Separation and contraction zones form in high velocity and low velocity areas in the bend, respectively. These separation and contraction zones are at risk of erosion and sedimentation. Figure 6 shows the relative error ($((V_{model} - V_{exp})/V_{exp}) \times 100$) of the longitudinal velocity contours predicted by the GP-Hybrid, GP-BP, SC-Hybrid and SC-BP models and experimental values with the test dataset in a 90° sharp bend. According to these figures, the error in the separation zone (left side of the plots) for all models is less than the contraction zone (right side of the plots). In the separation zone (at the inner wall), the GP-BP model produced greater error than the other models (by about 10%) and the GP-Hybrid

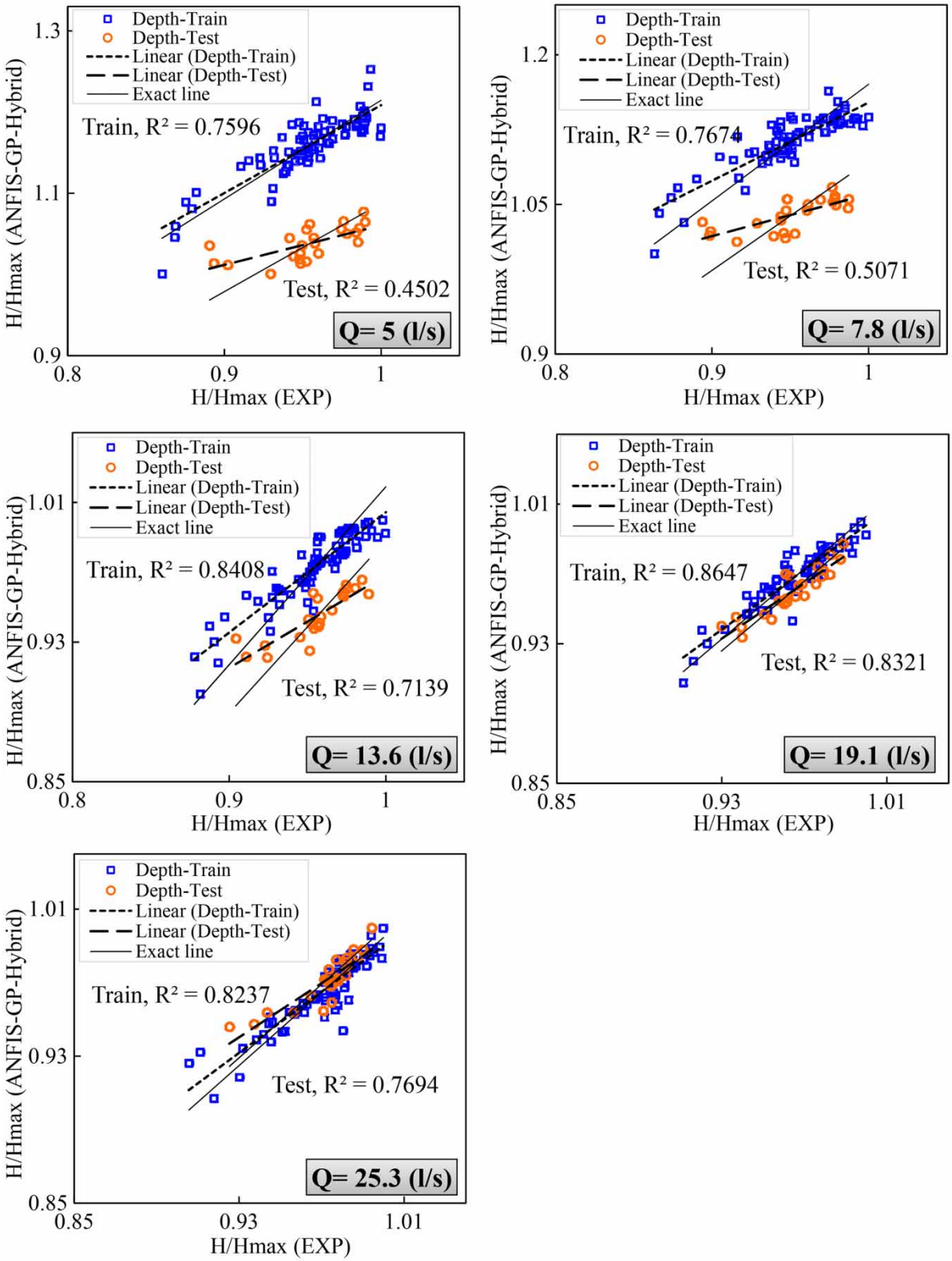

Figure 5 | Regression graphs of velocity values predicted by the GP-Hybrid, GP-BP, SC-Hybrid and SC-BP models compared with experimental results for the training and testing datasets.

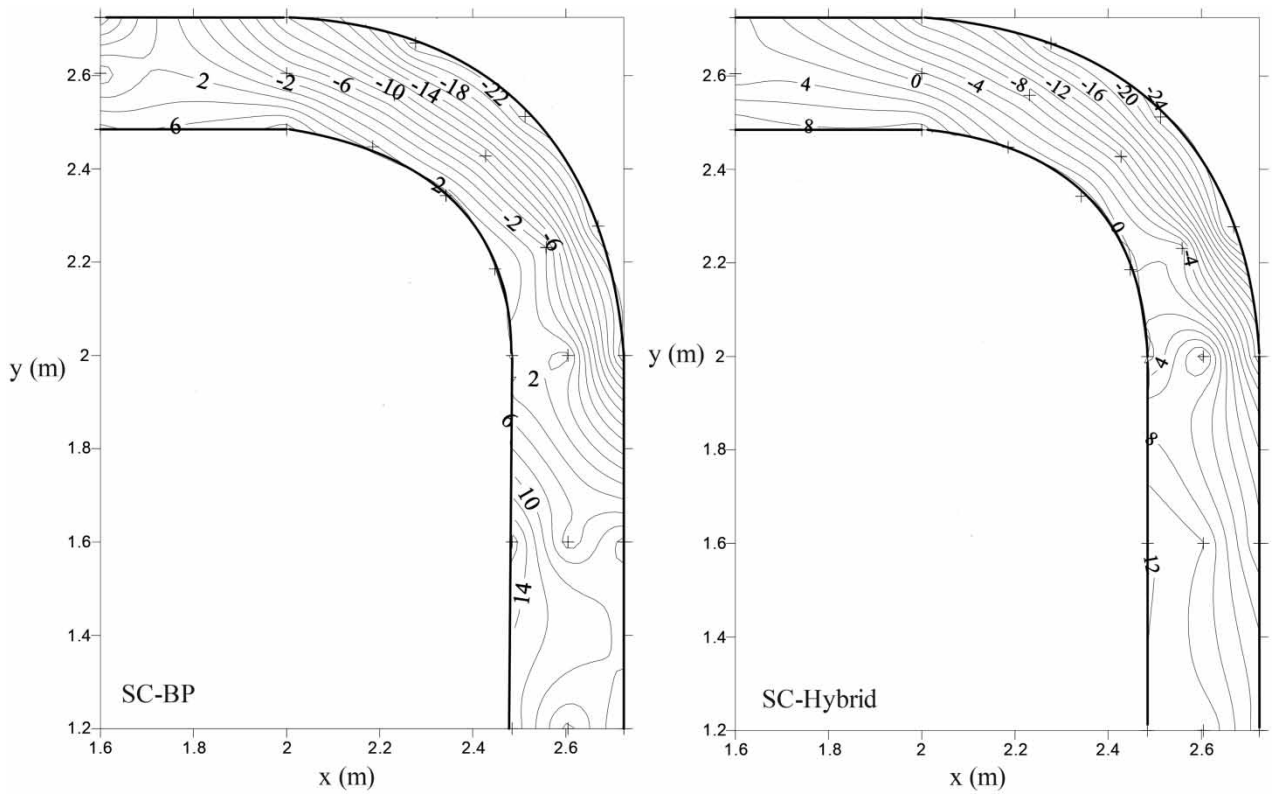

Figure 6 | Longitudinal velocity error values predicted by the GP-Hybrid, GP-BP, SC-Hybrid and SC-BP models compared with the experimental values in $((V_{model}-V_{exp})/V_{exp})\%$ for the test dataset.

was the most accurate in this area. Although all models behaved the same, the two hybrid GP and SC models had the lowest accuracy in the contraction zones (at the outer wall). The negative error percentages indicate that the velocity values predicted by the models are lower than the experimental values. The figures show that most errors of all four models were negative, and as a result, the models were partly affected by underestimation. The greatest error values of the GP-BP, GP-Hybrid, SC-BP and SC-Hybrid models were 22%, 30%, 22% and 24%, respectively. Two GP models with two different training algorithms were compared with two SC models in the areas after the bend. The GP models exhibited lower error with GP-BP and GP-hybrid errors of approximately 0 and 1%, while the error values of the two SC models in the areas after the bend were approximately 12–14%. The two SC models had the lowest error at the end cross sections of the bend (2–4%). In light of the sharp bend and the presence of secondary flows in the sections located after the bend, it can be concluded that the GP models predicted the velocity in these areas with lower error than the SC models. It can be said that the low error value of the GP-Hybrid model indicates good performance in velocity prediction. Therefore, the hybrid models improved BP model performance in the important areas of the bend (e.g. separation zones, after the bend, etc.), and their reduction of other bending effects (such as the presence of secondary flows after the bend) was very efficient.

CONCLUSION

In this study, the velocity and flow depth parameters in a 90° sharp bend were predicted using ANFIS models. In the ANFIS design, two methods were used for FIS generation, namely GP and a SC algorithm, while BP and a hybrid of BP and LS were used to train the models. Thus, ANFIS modeling of the velocity and flow depth parameters was done

with four different models: GP-BP, GP-Hybrid, SC-BP and SC-Hybrid. In each model, coordinates of 13 points in eight different cross sections and different discharge (Q) rates were considered as input parameters. The modeling results indicate that the velocity and flow depth prediction by the GP method in a 90° sharp bend was more accurate than SC for FIS generation. Additionally, for each velocity and flow depth prediction, the GP model with a hybrid of BP and LS training algorithm (R^2 of 0.867 and 0.998, respectively) outperformed the backpropagation algorithm. The error contours in the bend also show that all four models achieved the highest accuracy at the inner wall (separation zone) and lowest accuracy at the outer wall (contraction zone). For future work, it is recommended to build an ANFIS model using an evolutionary algorithm such as the GA and differential evolution and compare its performance to the model with BP and hybrid algorithm employed in this study.

REFERENCES

Akhtari, A. A., Abrishami, J. & Sharifi, M. B. 2009 Experimental investigations water surface characteristics in strongly-curved open channels. *Journal of Applied Sciences* **9**, 3699–3706.

Anwar, H. O. 1986 Turbulent structure in a river bed. *Journal of Hydraulic Engineering, ASCE* **112**, 657–669.

Asadiani Yekta, A. H., Marsooli, R. & Soltani, F. 2010 Suspended sediment estimation of Ekbatan Reservoir Sub Basin using adaptive neuro-fuzzy inference systems (ANFIS), artificial neural networks (ANN), and sediment rating curves (SRC). In: *Proceedings of the International Conference on Fluvial Hydraulics: River Flow* (A. Dittrich, K. Koll, J. Aberle & P. Geisenhainer, eds). Bundesanstalt für Wasserbau. 8–10 September, Braunschweig, Germany, pp. 807–813.

Baghalian, S., Bonakdari, H., Nazari, F. & Fazli, M. 2012 Closed-form solution for flow field in curved channels in comparison with experimental and numerical analyses and artificial neural network. *Engineering Applications of Computational Fluid Mechanics* **6**, 514–526.

Bahramifar, A., Shirkhani, R. & Mohammadi, M. 2013 An ANFIS-based approach for predicting the manning roughness coefficient in alluvial channels at the bank-full stage. *International Journal of Engineering* **26**, 177–186.

Barbhuiya, A. K. & Talukdar, S. 2010 Scour and three dimensional turbulent flow fields measured by ADV at a 90° horizontal forced bend in a rectangular channel. *Flow Measurement and Instrumentation* **21**, 312–321.

Bergs, M. A. 1990 Flow Processes in a Curved Alluvial Channel. PhD Thesis, University of Iowa, Iowa, USA.

Blanckaert, K. & Graf, W. H. 2001 Mean flow and turbulence in open channel bend. *Journal of Hydraulic Engineering, ASCE* **127**, 835–847.

Bodnar, T. & Prihoda, J. 2006 Numerical simulation of turbulent free-surface flow in curved channel. *Flow, Turbulence and Combustion* **76**, 429–442.

Bonakdari, H., Larrarte, F. & Joannis, C. 2007 Effect of a bend on the velocity field in a circular sewer with free surface flow. In: *Proceeding of 6th International Conference on Sustainable Techniques and Strategies in Urban Water Management*, Lyon, France, June 24–28, pp. 1401–1408.

Bonakdari, H., Baghalian, S., Nazari, F. & Fazli, M. 2011 Numerical analysis and prediction of the velocity field in curved open channel using artificial neural network and genetic algorithm. *Engineering Applications of Computational Fluid Mechanics* **5**, 384–396.

Bowden, G. J., Maier, H. R. & Dandy, G. C. 2002 Optimal division of data for neural network models in water resources applications. *Water Resources Research* **38**, 2-1–2-11.

Chau, K. W. & Wu, C. L. 2010 A hybrid model coupled with singular spectrum analysis for daily rainfall prediction. *Journal of Hydroinformatics* **12**, 458–473.

Chiang, Y. M., Chang, L. C. & Chang, F. J. 2004 Comparison of static-feedforward and dynamic-feedback neural networks for rainfall–runoff modeling. *Journal of Hydrology* **290**, 297–311.

Chiu, S. 1997 Extracting fuzzy rules from data for function approximation and pattern classification. In: *Fuzzy Information Engineering: a Guided Tour of Applications* (D. Dubois, H. Prade & R. Yager, eds). Springer, Berlin, Germany, pp. 149–162.

DeMarchis, M. & Napoli, E. 2006 3D numerical simulation of curved open channel flows. In: *Proceedings of 6th International Conference on Water Resources, Hydraulics & Hydrology*, Chalkida, Evia Island, Greece, pp. 86–91.

DeVriend, H. J. & Geoldof, H. J. 1983 Main flow velocity in short river bends. *Journal of Hydraulics Engineering* **109**, 991–1011.

Ebtehaj, I. & Bonakdari, H. 2013 Evaluation of sediment transport in sewer using artificial neural network. *Engineering Applications of Computational Fluid Mechanics* **7**, 382–392.

Ebtehaj, I. & Bonakdari, H. 2014 Performance evaluation of adaptive neural fuzzy inference system for sediment transport in sewers. *Water Resources Management* **28**, 4765–4779.

Ferguson, R. I., Parsons, D. R., Lane, S. N. & Hardy, R. J. 2003 Flow in meander bends with recirculation at the inner bank. *Journal of Water Resources Research* **39**, 1–13.

Gholami, A., Akhtari, A. A., Minatour, Y., Bonakdari, H. & Javadi, A. A. 2014 Experimental and numerical study on velocity fields and water surface profile in a strongly-curved 90° open channel bend. *Engineering Applications of Computational Fluid Mechanics* **8**, 447–461.

Gholami, A., Bonakdari, H., Zaji, A. H. & Akhtari, A. A. 2015 Simulation of open channel bend characteristics using

computational fluid dynamics and artificial neural networks. *Engineering Applications of Computational Fluid Mechanics* **9**, 355–369.

Gholami, A., Bonakdari, H., Zaji, A. H., Ajeel Fenjan, S. & Akhtari, A. A. 2016a Design of modified structure multi-layer perceptron networks based on decision trees for the prediction of flow parameters in 90° open-channel bends. *Engineering Applications of Computational Fluid Mechanics* **10**, 194–209.

Gholami, A., Bonakdari, H., Zaji, A. H., Michelson, D. G. & Akhtari, A. A. 2016b Improving the performance of multi-layer perceptron and radial basis function models with a decision tree model to predict flow variables in a sharp 90° bend. *Applied Soft Computing* **48**, 563–583.

Guven, A. & Gunal, M. 2008 Prediction of scour downstream of grade-control structures using neural networks. *Journal of Hydraulic Engineering, ASCE* **134**, 1656–1660.

Jang, J. S. R. 1993 ANFIS: adaptive-network-based fuzzy inference system. *IEEE Transactions on Systems, Management, and Cybernetics* **23**, 665–685.

Kennedy, P., Condon, M. & Dowling, J. 2003 Torque-ripple minimization in switched reluctant motors using a neuro-fuzzy control strategy. In: *Proceeding of the IASTED International Conference on Modeling and Simulation*, Palm Springs, USA.

Leschziner, M. A. & Rodi, W. 1979 Calculation of strongly curved open channel flow. *Journal of the Hydraulics Division* **105**, 1297–1314.

Lien, H. C., Hsieh, T. Y., Yang, J. C. & Yeh, K. C. 1999 Bend flow simulation using 2D depth-averaged model. *Journal of Hydraulic Engineering, ASCE* **125**, 1097–1108.

Liriano, S. L. & Day, R. A. 2001 Prediction of scour depth at culvert outlets using neural networks. *Journal of Hydroinformatics* **3**, 231–238.

Moharana, S. & Khatua, K. K. 2014 Prediction of roughness coefficient of a meandering open channel flow using neuro-fuzzy inference system. *Measurement* **51**, 112–123.

Naji, M. A., Ghodsian, M., Vaghefi, M. & Panahpur, N. 2010 Experimental and numerical simulation of flow in a 90° bend. *Flow Measurement and Instrumentation* **21**, 292–298.

Ramamurthy, A., Han, S. & Biron, P. 2013 Three-dimensional simulation parameters for 90° open channel bend flows. *Journal of Computing in Civil Engineering* **27**, 282–291.

Rozovskii, I. L. 1961 *Flow of Water in Bends of Open Channels*. Academy of Sciences of the Ukrainian SSR, Israel Program for Science Translation. Jerusalem, Israel.

Sahu, M., Jana, S., Agarwal, S. & Khatua, K. K. 2011 Point form velocity prediction in meandering open channel using artificial neural network. In: *2nd International Conference on Environmental Science and Technology*, IACSIT Press, Singapore, 6, pp. 209–212.

Samandar, A. 2011 A model of adaptive neural-based fuzzy inference system (ANFIS) for prediction of friction coefficient in open channel flow. *Scientific Research and Essays* **6**, 1020–1027.

Shukry, A. 1950 Flow around bends in an open flume. *Transactions-ASCE* **115**, 751–788.

Steffler, P. M., Rajartnam, N. & Peterson, A. W. 1985 Water surface change of channel curvature. *Journal of Hydraulic Engineering, ASCE* **111**, 866–870.

Uddin, M. N. & Rahman, M. M. 2012 Flow and erosion at a bend in the braided Jamuna River. *International Journal of Sediment Research* **27**, 498–509.

Vaghefi, M., Akbari, M. & Fiouz, A. R. 2015 Experimental investigation of the three-dimensional flow velocity components in a 180° sharp bend. *World Applied Programming* **5**, 125–131.

Wang, W. C., Chau, K. W., Xu, D. M. & Chen, X. Y. 2015 Improving forecasting accuracy of annual runoff time series using ARIMA based on EEMD decomposition. *Water Resources Management* **29**, 2655–2675.

Yager, R. R. & Filev, D. P. 1994 Approximate clustering via the mountain method. *IEEE Transactions on Systems, Management, and Cybernetics* **4**, 1279–1284.

Ye, J. & McCorquodale, J. A. 1998 Simulation of curved open channel flows by 3D hydrodynamic model. *Journal of Hydraulic Engineering, ASCE* **124**, 687–698.

Yuhang, Z. & Wenxin, H. 2009 Application of artificial neural network to predict the friction factor of open channel flow. *Communications in Nonlinear Science and Numerical Simulation* **14**, 2373–2378.

Zeng, J., Constantinescu, G., Blanckaert, K. & Weber, L. 2008 Flow and bathymetry in sharp open-channel bends: experiments and predictions. *Water Resources Research* **44**, w09401.

First received 29 September 2015; accepted in revised form 24 January 2017. Available online 6 March 2017